processes

MDPI

Article

Investigation of Thermal Radiation from Soot Particles and Gases in Oxy-Combustion Counter-Flow Flames

Chaoyang Wang [1], Guangtong Tang [1], Huibo Yan [1], Lujiang Li [1], Xiaopei Yan [1], Zhicong Li [2] and Chun Lou [2,*]

[1] State Grid Hebei Energy Technology Service Co., Ltd., Shijiazhuang 050021, China; dyy_wangcy@he.sgcc.com.cn (C.W.); dyy_tanggt@he.sgcc.com.cn (G.T.); dyy_yanhb@he.sgcc.com.cn (H.Y.); dyy_lilj@he.sgcc.com.cn (L.L.); dyy_yanxp@he.sgcc.com.cn (X.Y.)

[2] State Key Laboratory of Coal Combustion, School of Energy and Power Engineering, Huazhong University of Science and Technology, Wuhan 430074, China; lzc97@hust.edu.cn

* Correspondence: Lou_chun@sina.com or clou@hust.edu.cn; Tel.: +86-136-1863-9018

Abstract: Oxy-combustion with high flame temperature, low heat loss, high combustion efficiency, and low NOx emissions is being extensively studied. The thermal radiation from soot particles and gases in oxy-combustion accounts for the vast majority of the total heat transfer. Based on a detailed chemical reaction mechanism coupled with the soot particle dynamics model and optically thin radiation model, the influence of the flame structure and temperature distribution on the thermal radiation in oxygen-enriched counterflow diffusion flames was studied in this paper. The results revealed that reasonable assignment of total recycled flue gas and the degree of dilution of fuel and oxidant were critical, which can be used to adjust the overall radiation situation of the flame. At the same adiabatic flame temperature, as the fuel concentration decreased and the oxidant concentration increased (the stoichiometric mixture ratio is from 0.3 to 0.6), the soot formation decreased, which led to the particle radiation disappearing while the main radiation zone of gases moved 0.04 cm toward the fuel side. At the same stoichiometric mixture fraction (0.4), the radiation area was broadened and the radiation of soot particles was gradually enhanced with the adiabatic flame increasing from 2300 K to 2700 K.

Keywords: oxy-combustion; recycled flue gas; radiation; temperature distribution; flame structure

Citation: Wang, C.; Tang, G.; Yan, H.; Li, L.; Yan, X.; Li, Z.; Lou, C. Investigation of Thermal Radiation from Soot Particles and Gases in Oxy-Combustion Counter-Flow Flames. *Processes* **2021**, *9*, 1756. https://doi.org/10.3390/pr9101756

Academic Editors: Albert Ratner and Zhihua Wang

Received: 13 July 2021
Accepted: 28 September 2021
Published: 30 September 2021

1. Introduction

Traditional coal-fired boilers use air for combustion, in which N_2 in the air (approximately 79% by volume) dilutes CO_2 in the flue gas. The resulting low concentration of CO_2 in the flue gas makes it extremely difficult to capture and recover CO_2. Oxy-combustion technology is considered an effective technology that can solve this problem, by enhancing the oxygen concentration and using recycled flue gas (RFG) [1–4]. Oxy-combustion technology can be used to obtain a high concentration of CO_2 in the products of the combustion system, which is beneficial to the storage and utilization of CO_2. With the development of gas recirculation technology, many concepts of oxy-combustion based on RFG have been proposed. RFG (mainly CO_2) is used as a dilution gas to control the structure, temperature, and heat flux of the flame, and has been widely used in gas turbines and coal-fired power plants [5].

Through the transformation of the combustion system, RFG emissions can be significantly reduced, combustion efficiency can be improved, and pollutants emission costs can be reduced [6,7]. However, the increase of oxygen concentration and the decrease of fuel dilution in the diffusion flame will lead to the increase of flame temperature and soot concentration, and soot particles are emitted [8,9]. As soot particles are harmful to the environment and the human body, it is very important to understand the effects of RFG on soot formation and oxidation in the oxy-combustion system and also to further control the radiation from soot particles in flames [10]. Due to the necessity for soot research, many

studies have measured the soot volume fraction in flames through experiments [11,12], and studied the effects of oxygen concentration and CO_2 on soot formation characteristics in flames [13–17]. In addition, changing the structure of the flame (changing the concentration of the inert gas in the oxidant and fuel) can significantly change the soot formation and oxidant characteristics of the flame, and the bright yellow flame, which is full of soot particles, can be changed to a blue flame with radical chemiluminescence, even in the case of adiabatic flame temperature (T_{ad}) constant. This phenomenon has been observed in many types of non-premixed flames, such as counterflow flames [13–15] and laminar coflow diffusion flames [16,17]. The stoichiometric mixture fraction (Z_{st}) to describe the flame structure and the degree of dilution of the fuel and oxidant can be introduced as:

$$Z_{st} = (1 + Y_{F,0} W_O \upsilon_O / Y_{O,0} W_F \upsilon_F)^{-1} \quad (1)$$

where Y_0 is the mass fraction at the system boundary, W is the molecular mass, and υ is the stoichiometric coefficient. The subscripts F and O are fuel flow and oxidant flow, respectively. Changing Z_{st} can influence the temperature, composition distribution, and soot yield, which ultimately affect the heat flow distribution.

Atreya et al. studied thermal radiation and soot particulate emission in partially premixed counterflow flames [18]. Experimental results have found that the configuration of the soot zone spatially entrained between the premixed and non-premixed reaction zones may enhance radiative heat transfer while reducing soot emissions. Liu et al. studied the effects of gas and soot radiation in a counterflow ethylene diffusion flame by using the semiempirical two-equation soot model and the radiation heat transfer model calculated by the DOM/SNBCK method and found that gas radiation is more important than soot radiation in influencing the flame temperature and soot volume fraction (SVF) [19]. Based on the soot volume fraction per unit, soot radiation in a counterflow diffusion flame is less important than that in a coflow flame. Due to the gas radiation in the peak flame temperature region and the soot radiation at a much lower temperature, the distribution of the radiation source term presents a double valley structure. In O_2/N_2 and O_2/CO_2 atmospheres, Guo et al. studied the influence of the Z_{st} flame structure on the combustion characteristics of different ethylene counterflow diffusion flames, through a variety of designed flames [14], which isolated the temperature and dilution degree effects. They found that with the increase in Z_{st}, using N_2 or CO_2 as a diluent can inhibit the formation of soot, and that compared to N_2, the effect of CO_2 on the inhibition of soot formation is more obvious.

In summary, the flame temperature distribution and flame structure changes could affect the formation of soot and the spatial distribution of the radiation medium, and then ultimately affect the overall thermal radiation of the flame. We will use pure CO_2 here instead of a more complex RFG for diluting fuel and oxidant to obtain different T_{ad} and flame structures. The spatial distribution of radiation medium, including gases and soot particles, and the overall radiation of the flame in oxygen-enriched counterflow diffusion flame is studied by numerical calculations coupled with a detailed chemical reaction mechanism, soot particle dynamics model, and radiation model. These fundamental oxy-combustion studies shed light on how best to utilize RFG to control the flame temperature, SVF, and heat flux, to achieve savings in fuel and oxygen resources and obtain the best working conditions.

2. Numerical Methods

Numerical simulations of counterflow flames were carried out using the OPPDIF program, transport properties were obtained from the CHEMKIN database [20,21] and T_{ad} was calculated using NASA's Chemical Equilibrium with Applications program [22]. Cylindrical coordinates were selected. The tolerance of the solver was set to 1×10^{-10}, and the relaxation factor in segregated scheme was 0.7. The following describes the soot model and the radiation model used in the calculation.

2.1. Soot Model

The formation of soot particles includes a series of complex physical and chemical processes, which are generally divided into two processes including gas-phase reaction kinetics and the evolution of particle dynamics after nucleation, corresponding to the formation of precursor, particle nucleation, and subsequent growth, and evolution, respectively. The gas-phase reaction process is studied by a detailed chemical reaction mechanism, while the evolutionary process of soot particles is described by soot aerosol dynamics models. In this paper, ethylene was chosen as the fuel; the C_2H_4 combustion mechanism comes from Appel et al. [23,24], and consists of fuel pyrolysis, C0-C4 small molecule core reaction, initial benzene ring formation, polycyclic aromatic hydrocarbons (PAHs) formation, and growth reactions up to pyrene (A4), then soot particles are created by the dimerization of A4. Soot particles growth mainly involves the H-abstraction-C_2H_2-addition (HACA) process and PAH condensation [23,25]. The method of sectional was used to solve the particles equations. 25 sections were set, the spacing factor was 2.0, and the section minimum size was 32. The coagulation collision efficiency was set to 2.2, and the diffusion and thermophoresis of the particles were considered.

2.2. Radiation Model

Gases and soot particles radiations are the main ways of flame radiation heat transfer; therefore, it is important to couple them with an appropriate radiation model. Considering that the flame optical thickness is generally thin (in millimeter orders of magnitude) in counterflow diffusion flames, only the thermal radiation to the outside of the flame was calculated and the internal reabsorption of the flame can be ignored. The radiation heat-transfer model used an optically thin media radiative transmission; the radiation medium included gas (CO_2, CO, H_2O, and CH_4) and soot particles. The flame radiation was calculated by adding the radiation source to the energy equation, and the radiative heat transfer by soot, CO_2, H_2O, CO, and CH_4 were calculated using an optically thin radiation model with the Planck mean absorption coefficient. The Planck mean absorption coefficients for species i (i = CO_2, H_2O, CH_4, and CO) used when calculating the optically thin radiation heat loss were obtained by the RADCAL method [26,27], while the mean absorption coefficient for the particles was calculated by $k_{\mathrm{par}} = 1862 * f_{\mathrm{v}}T$ [28]. Meanwhile, it was assumed that the local gas and the soot particles had the same temperature locally.

3. Model Verification and Flame Design

Before conducting the oxy-fuel flame calculations, the correctness of the numerical model was first verified. Based on the location of the stagnation plane, the counterflow flames can be divided into soot-formation (SF) flames and soot-formation–oxidation (SFO) flames [29]. SF flames usually mean that the flame sheet is located on the oxidant side of the stagnation plane, and it is usually a counterflow flame with pure fuel and low oxygen concentration. The flame sheet of SFO is on the fuel side of the stagnation plane, which is achieved by setting high fuel dilution and high oxygen concentration. As a result, we conducted model verifications on the two types of counterflow flames. For SF, we set the same conditions as in [30] for the C_2H_4 counterflow diffusion flames. The separation distance between the nozzles was 1.42 cm, the fuel stream was pure C_2H_4 for the non-diluted flame and the oxidant stream consisted of 24% O_2 and 76% N_2 by volume. To keep the overall strain rate constant, the nozzle exit velocities of the fuel and oxidant streams were maintained at 19.5 cm/s. At the same time, N_2 in oxidant streams was replaced with CO_2 under the same conditions to initially explore the difference between N_2 and CO_2 on the impact of temperature field, soot particle distribution, heat release or transmission, and so on. Figure 1 shows the computed and experimental SVFs and temperature profiles. Experimental and calculated peak values of SVF are 1.67 ppm and 1.48 ppm, respectively. The locations of peak SVF of the two differ by about 0.3 cm, and the calculated sooting zone is narrower than the experimental one, which may be because the numerical model of this manuscript does not have a good prediction of the thermophoresis and diffusion of

soot particles, which are exactly responsible for the wide range of soot volume fraction in the experimental flame. The peak temperatures and distributions are consistent.

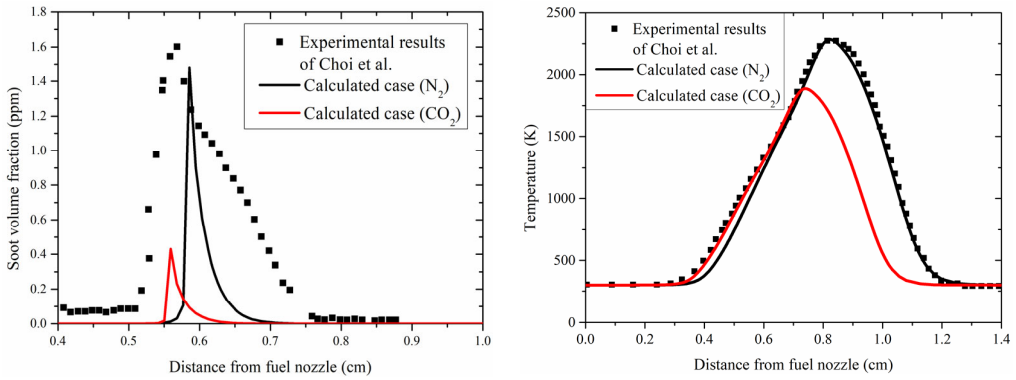

(**a**) (**b**)

Figure 1. Calculated and experimental SVF profiles (**a**) and temperature profiles (**b**) of SF flames.

CO_2 replaces N_2 as dilution progresses, showing significant impacts on the temperature field, soot particle formation or distribution, heat release, and heat radiation. In Figure 1a, the peak value of SVF in the CO_2/O_2 atmosphere is about 0.43 ppm, only a quarter of the value in the N_2/O_2 atmosphere. Figure 2a shows the net heat generated by the reaction and the temperature distribution in N_2/O_2 and CO_2/O_2 atmospheres; the $C_2H_4/O_2 + CO_2$ counterflow diffusion flame has more net heat production from gas-phase reactions than the $C_2H_4/O_2 + N_2$ flame, because CO_2 is not an absolutely inert gas, it participated in some chemical reactions, especially in some exothermic reactions [3]. Figure 2b is the radiation source from soot particles and gases (CO_2, H_2O, CO, and CH_4). The radiation source of the N_2/O_2 atmosphere generates two valleys. The valley at a distance of 0.6 cm from the fuel nozzle is caused by the radiation of soot, which corresponds to the peak soot position in Figure 1a. The valley at 0.8 cm is due to the peak temperature, which greatly enhances the gas radiation. However, due to low-yield soot particles and high concentration of CO_2, the radiation from the particles can be ignored compared to gas radiation in the CO_2/O_2 atmosphere. The sudden increase in CO_2 concentration leads gas radiation to become the most important radiation source.

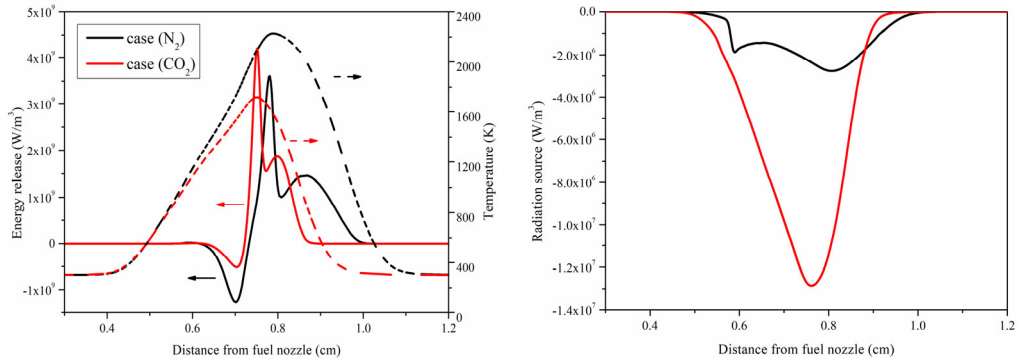

(**a**) (**b**)

Figure 2. Heat generated by the reaction and temperature distribution (**a**) and radiation source (**b**) in N_2 and CO_2 atmospheres.

For the SFO flames, the separation distance between the nozzles was 8 mm, the oxidant stream was composed of 90% O_2 and 10% N_2 by volume, and the fuel stream was composed of 28% C_2H_4 and 72% N_2. The nozzle exit velocities of the fuel and oxidant streams were maintained at 20 cm/s [31]. The comparison between the experimental and calculated SVF of the SFO flame is shown in Figure 3. The experimental and calculated peak values by

Xu et al. were 0.21 ppm and 0.19 ppm, respectively, while the calculated peak SVF of this study was 0.189 ppm, and the peak position was relatively close. The results show that for the SFO flame with a high oxygen concentration and a high fuel dilution, this numerical model can accurately predict experimental results.

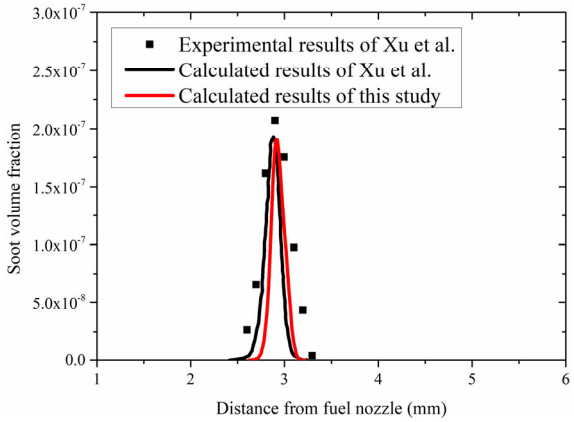

Figure 3. Calculated and experimental SVF profiles of SFO flames.

Overall, even if there is a difference in the sooting zone for SF flames, the peak values and positions are worthy of attention in the discussion of the results. In addition, SFO can be accurately simulated, so the model verification shows that this numerical model can be better used to predict and characterize the counterflow diffusion flame, especially in the conditions of fuel dilution and oxygen enhancement.

Here, three groups of flame were designed after comprehensive consideration, in which CO_2 was used as a diluent, to research the effects of flame structure and T_{ad} on soot formation and on radiation from gases and soot. Each group maintained a constant T_{ad} with Z_{st} increasing, but the T_{ad} of each group was different. The flame cases were designed to simultaneously dilute both sides of the fuel stream and oxidant stream with a diluent gas, while ensuring that the total stoichiometric amount of CO_2 per group was unchanged, so T_{ad} was unaffected. The two nozzles of the burner were coaxial and flowed in opposite directions, with a diameter of 10 mm and a separation distance of 8 mm. The initial velocity of the reactant from the nozzle was maintained at 20 cm/s to ensure that the global strain rate remained nearly constant (50 s^{-1}). The initial temperatures of the fuel stream, the oxidant stream, and the ambient temperature all were maintained at 300 K, and the pressure was 1 atm. Table 1 displays the details of the designed flames.

Table 1. Three groups of cases used in our numerical calculations.

Case	X_{O2}	Z_{st}	Y_O	Y_F	T_{ad} (K)
1.1	31.65%	0.10	0.252	0.665	2300
1.2	35.21%	0.20	0.283	0.332	
1.3	39.68%	0.30	0.324	0.221	
1.4	45.46%	0.40	0.377	0.166	
2.1	49.18%	0.30	0.413	0.285	2500
2.2	56.18%	0.40	0.482	0.212	
2.3	65.50%	0.50	0.580	0.169	
2.4	78.53%	0.60	0.727	0.141	
3.1	70.42%	0.40	0.634	0.280	2700
3.2	81.97%	0.50	0.768	0.221	
3.3	96.78%	0.60	0.956	0.185	
3.4	100.00%	0.62	1.000	0.180	

4. Results and Analysis

As a general rule, a permanent blue flame can be obtained when there is no soot present (which leads to visible radiation) in the flames. With the increase of soot, the flames gradually change from pure blue to yellow (soot radiation), or even bright white. Therefore, the incipient soot formation was studied by varying the mole fraction of oxygen in the oxidant stream for a given mole fraction of fuel in the fuel stream, similar to the definition of Z_{st}. Incipient soot formation is generally referred to as the sooting limit, which has been studied by many scholars, especially in diffusion flames [32–34]. Figure 4 shows the three calculated iso-T_{ad} (solid lines) and six calculated iso-Z_{st} (dotted lines) curves in the O_2/CO_2 atmosphere, highlighting that flames with a lower T_{ad} have larger ranges of Z_{st}, corresponding to more varied flame structures. For instance, Z_{st} ranges from 0.0662 to 0.7732 in the first group (T_{ad} = 2300 K), whereas the range of variation of Z_{st} is reduced from 0.0846 to 0.7098 in the second group (T_{ad} = 2500 K), and further narrowed from 0.1113 to 0.6184 in the last group (T_{ad} = 2700 K). In other words, the iso-Z_{st} is getting denser as T_{ad} gradually decreases.

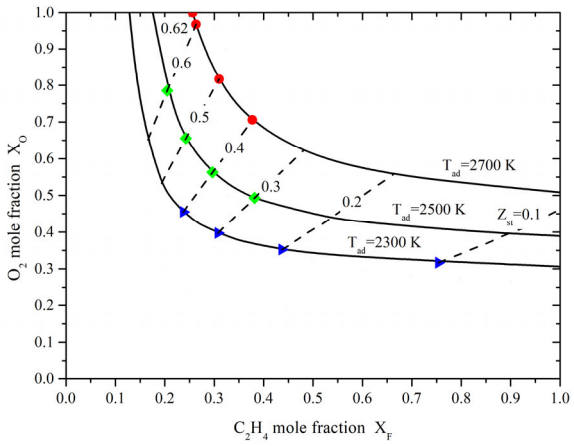

Figure 4. Iso-T_{ad} and iso-Z_{st} curves in O_2/CO_2 atmosphere.

4.1. Position Changes of Flame Sheet and Stagnation Plane

It is generally believed that the change in Z_{st} is mainly due to the change of position of the flame sheet and stagnation plane [29,31], which in turn affects the formation process of soot particles. Figure 5 shows the variation of the flame sheet position relative to the stagnation plane location in the conditions from Table 1. The abscissa is the difference between the flame sheet position and the stagnation plane location (from the fuel side), the ordinate is the stoichiometric mixed fraction Z_{st}.

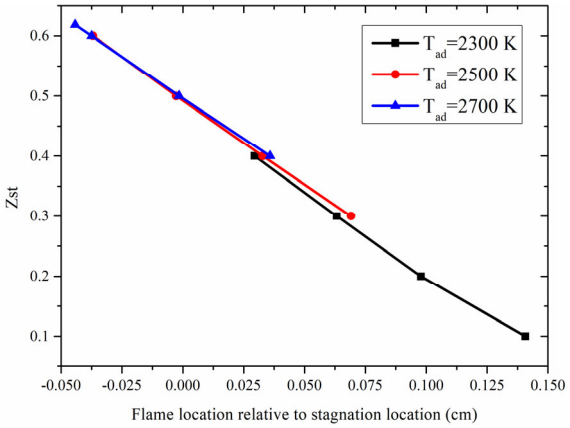

Figure 5. The variation of the relative position of the flame sheet and the stagnation plane in the calculated 3 × 4 conditions.

When Z_{st} is small (Z_{st} = 0.1–0.4), the flame sheet is located on the oxidant side of the stagnation plane. At that time, the fuel flowing out of the fuel side nozzle is continuously pyrolyzed in the process of approaching the stagnation plane. After reaching the stagnation plane, a portion of the species appearing across the stagnation plane through a diffusion mechanism then participate in the reaction with the oxidant. At the same time, the small molecular substances produced by the pyrolysis of the fuel react with each other while moving toward the stagnation plane to produce C_2H_2, C_3H_3, n-C_4H_i, etc. A1 appears and grows up to A4, and then the soot particles are born and grown; eventually, the soot particles are pushed toward the stagnation plane by the gas flow. In this situation, the entire evolution of the soot particles is carried out on the fuel side of the flame sheet and does not pass through the highly oxidizing flame sheet, so the soot particle only grows and is not being consumed by oxidation.

As the Z_{st} increases, the oxygen concentration in the oxidant gradually increases; the stagnation plane and flame sheet, which are relatively distant from each other at first, become close to each other and then gradually separate. In other words, the stagnation plane moves toward the oxidant side and the flame sheet moves continuously toward the fuel side. When the flame sheet moves to the fuel side of the stagnation plane (e.g., Z_{st} = 0.6), the fuel flowing out of the fuel side nozzle has to pass through the flame sheet first in the process of approaching the stagnation plane, and so a large number of OH radicals with strong oxidation are found near the flame sheet, due to the increase in oxygen concentration. All of these inhibit the production of C_2H_2, PAHs, and other substances, as well as the inception and growth of soot particles, and other processes, resulting in a significant reduction in the number of soot particles reaching the stagnation plane.

4.2. Effects of Flame Structure on Radiation

First, the maximal soot particle number density is showed in Figure 6. All groups show the same pattern of soot with increasing Z_{st}, so the second group (T_{ad} = 2500 K) was selected for a more detailed analysis.

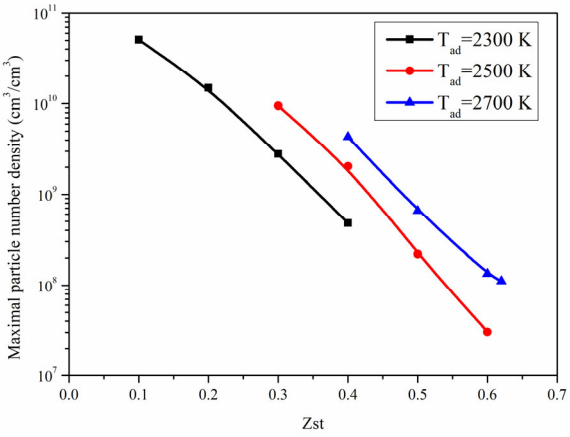

Figure 6. The maximal particle number density in the calculated 3 × 4 conditions.

Figure 7 shows the distributions of SVF and radiation source caused by soot and gases in cases 2.1–2.4. The peak of SVF in case 2.1 is about 0.23 ppm, while SVF is magnified by a factor of 100 in case 2.4 and almost no soot formation is predicted. With Z_{st} increasing (ranging from 0.3 to 0.6), the peak value of the radiation source increases gradually, but not obviously, and the overall position progressively approaches the fuel side (from 0.43 to 0.39 cm). There is also a lower peak in the radiation source curve of case 2.1, which is the contribution of radiation from the soot particles. However, compared to gas radiation, soot particle radiation is very weak. With Z_{st} increasing, soot formation is reduced and the contribution of radiation is almost negligible.

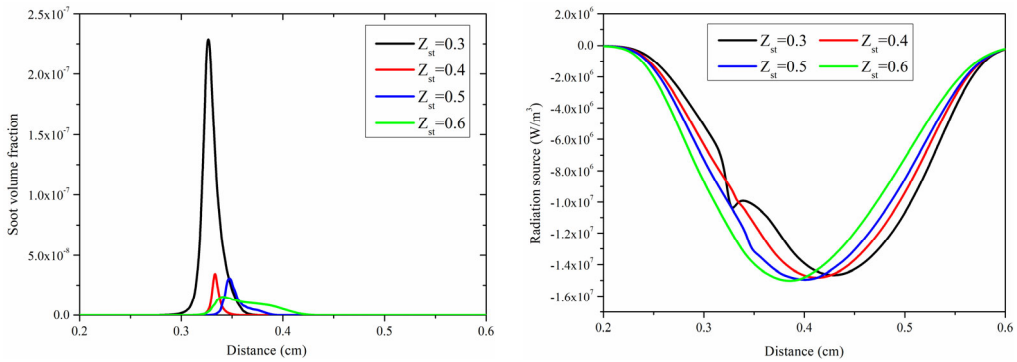

Figure 7. The distributions of SVF (**a**) and radiation source (**b**) in cases 2.1–2.4.

As mentioned earlier in this article, the soot particle growth mechanism mainly involves the HACA process and PAH condensation; soot particles are created by the dimerization of pyrene (A4) molecules, hydroxyl (OH) is mainly responsible for the oxidation and consumption of soot particles. We show the concentration distribution of several components, including C_2H_2, OH, A1 and A4 in Figure 8. An increase in the stoichiometric mixing fraction causes the concentration of fuel to be diluted and increases the oxygen concentration of oxidants.

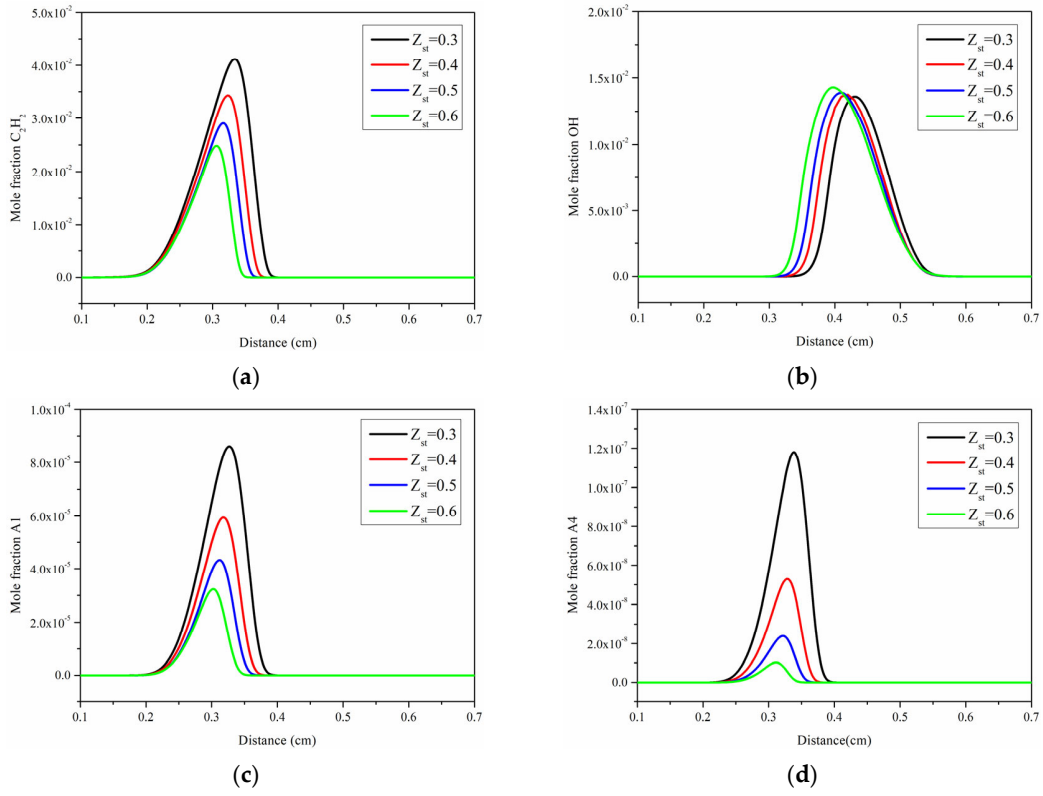

Figure 8. The mole fraction distributions of C_2H_2 (**a**), OH (**b**), A1 (**c**), and A4 (**d**) in cases 2.1–2.4.

Figure 9 shows the distributions of temperature (a), heat generation (b), CO_2 mole fraction (c), and H_2O mole fraction (d) in cases 2.1–2.4. The peak temperature and the distribution of the temperature field do not differ much when Z_{st} varies from 0.3 to 0.6, while the high-temperature zone moves about 0.01 cm toward the fuel side. Figure 9b shows the heat generation profiles of the group flames (cases 2.1–2.4) in different Z_{st}; the total energy release can be divided into three different regions: the endothermic fuel pyrolysis zone, the primary reaction zone near the maximum peak, and the secondary

oxidation zone near the second peak. The peak in the secondary oxidation zone gradually fades with the increase of Z_{st}, because the pyrolysis zone becomes narrower and the peak of the endothermic fuel pyrolysis zone decreases. The radiation heat source of soot particles and gas is consistent with that of Figure 7.

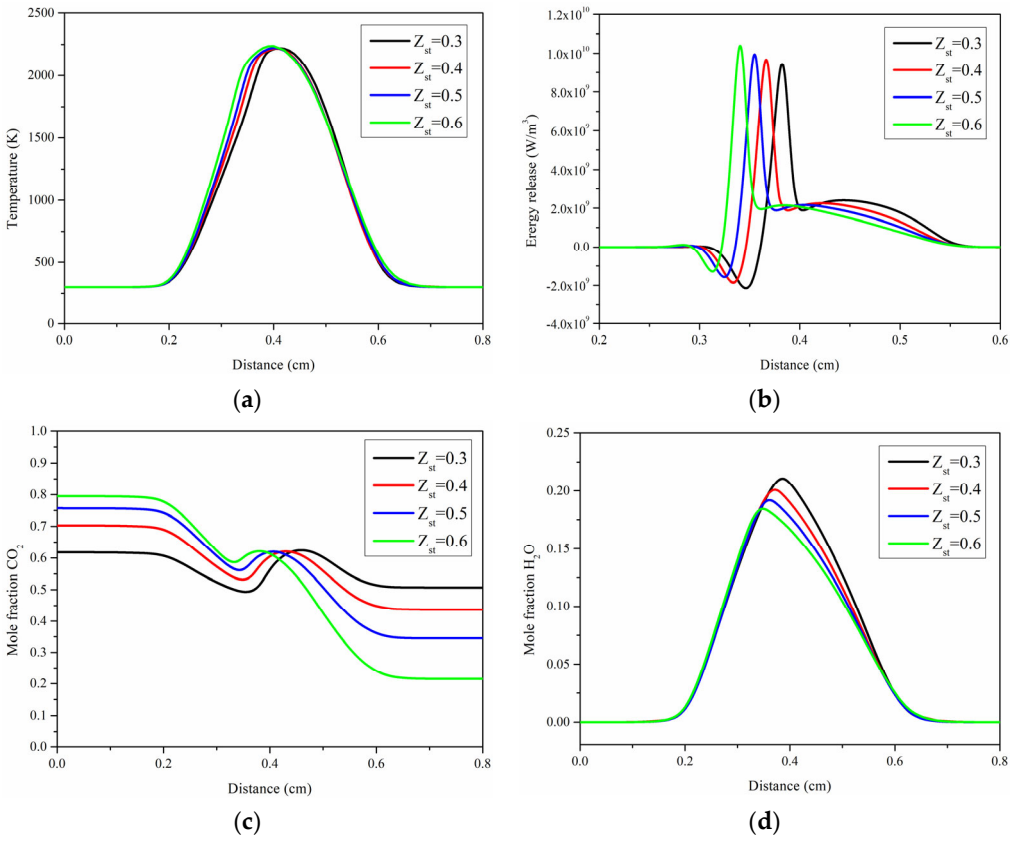

Figure 9. The distributions of temperature (**a**), heat generation (**b**), CO_2 mole fraction (**c**), and H_2O mole fraction (**d**) in cases 2.1–2.4.

Since CO_2 is required to dilute fuel and oxygen at the same time, with the increase of Z_{st}, more and more CO_2 is transferred from the oxidant side to the fuel side (the peak position has moved about 0.08 cm), making the four conditions in the boundary conditions of CO_2 concentration change significantly. The concentrations of CO_2 in the distributions vary widely in the nonreaction zone, hardly affecting radiation, while in the high-temperature reaction zone, the concentration of CO_2 changes very little with Z_{st} changing. At the same time, the H_2O in all conditions is generated only in the reaction without external introduction. The trend of the distribution of concentrations of H_2O in the four cases remains essentially unchanged; the peak value gradually decreases (the peak H_2O concentration at Z_{st} = 0.6 is 12.4% lower than that at Z_{st} = 0.3) and the position moves closer to the fuel side (from 0.386 to 0.349 cm).

4.3. Effects of Temperature Distribution on Radiation

Cases 1.4, 2.2, and 3.1 have different T_{ad} of 2300 K, 2500 K, and 2700 K, respectively, but all the flames have the same Z_{st} (0.4).

Figure 10 shows the SVF distributions and radiation source caused by soot and gases in cases 1.4, 2.2, and 3.1. With the increase of T_{ad}, soot formation gradually increases (from 0.019 to 0.205 ppm) and the distance between the peak SVF and the fuel nozzle drops from 0.35 to 0.315 cm. In Figure 10, we note a lower peak in the radiation source curve of case 3.1 contributed by soot particles. It was found that the gas radiation did not change significantly with the increase of temperature, because the Planck mean absorption coefficient for CO_2 gradually decreased [35], while the radiation distribution area gradually widened.

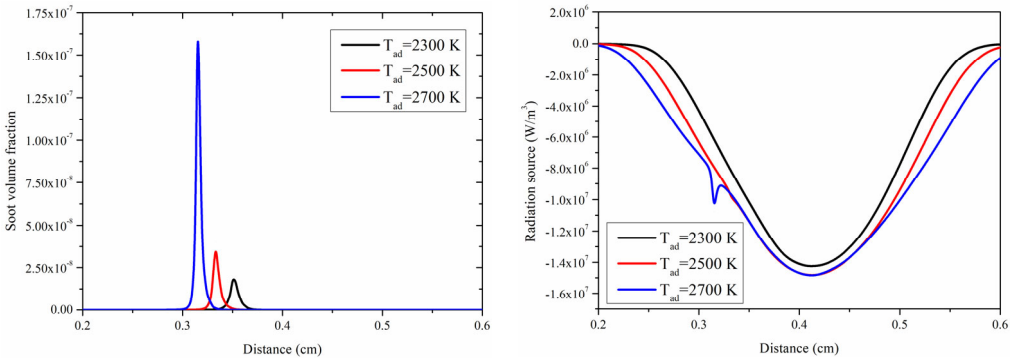

Figure 10. The distributions of SVF (**a**) and radiation source (**b**) in cases 1.3, 2.2, and 3.1.

Figure 11 shows the mole fraction distributions of C_2H_2, OH, A1, and A4 in cases 1.4, 2.2, and 3.1. On the whole, whether it is conducive to the growth of soot (C_2H_2, A1, and A4 species), or not (OH species), the molar concentration of species increases with the increase of temperature. This shows that the formation and oxidation of soot particles are accelerated simultaneously; however, compared to the oxidation rate of soot, its formation rate is faster.

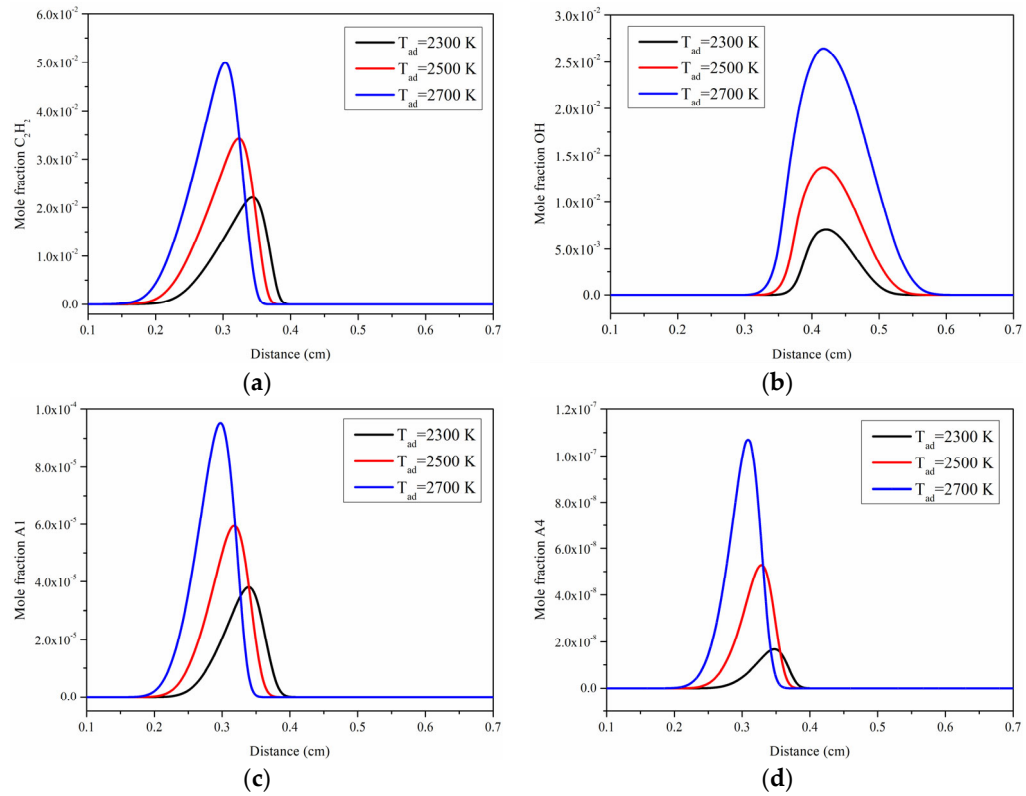

Figure 11. The mole fraction distributions of C_2H_2 (**a**), OH (**b**), A1 (**c**), and A4 (**d**) in cases 1.3, 2.2, and 3.1.

Figure 12 shows the distributions of temperature (a), heat generation (b), CO_2 mole fraction (c), and H_2O mole fraction (d) in cases 1.4, 2.2, and 3.1. The temperature area does not move significantly (about 0.4 cm), while the temperature increases significantly with a decrease in the total amount of CO_2 (for every 200 K increase in T_{ad}, the peak temperature increases by about 300 K). With a decrease in the total amount of CO_2 as a diluent, more fuel and oxidant are involved in reaction per unit volume, including pyrolysis of the fuel; in other words, more fuel is pyrolyzed and more heat is released, and

eventually, the temperature of the flame becomes higher by unit volume as demonstrated in Figure 12b.

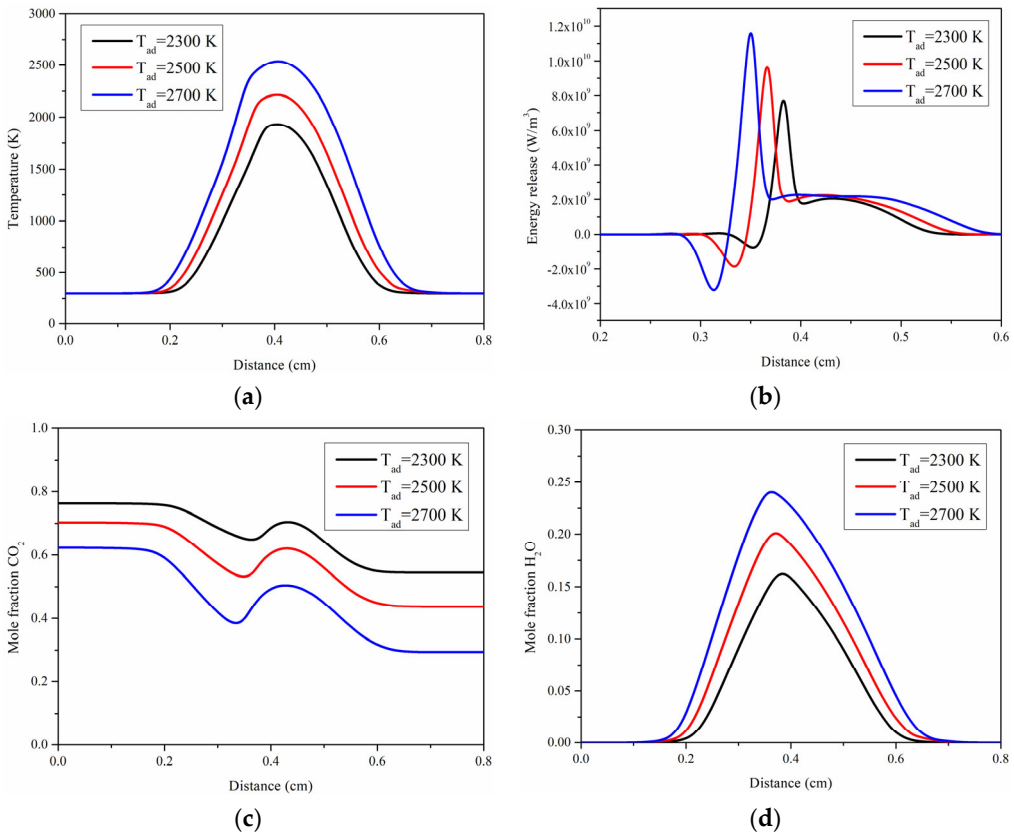

Figure 12. The distributions of temperature (**a**), heat generation (**b**), CO_2 mole fraction (**c**), and H_2O mole fraction (**d**) in cases 1.3, 2.2, and 3.1.

Due to the highly strained nature of the counterflow flame, soot formation is low, compared to the coflow and other flames, such as flames in the actual coal-fired boiler, so the radiation from particles would change violently with the amount of RFG. Therefore, it must be emphasized that the practice of reducing the amount of RFG requires more experimental and theoretical research.

5. Conclusions

In this paper, the effects of flame structure and temperature distribution on the radiation emission of soot particulate matter and gases in oxygen-enriched counterflow diffusion flame were studied by coupling a detailed chemical reaction mechanism with soot and radiation models. The first calculation indicated that under the same conditions, although CO_2 can inhibit the formation of soot due to its strong radiation properties, the overall radiation heat does not fall but instead rises. At the same T_{ad}, the fuel concentration decreases and the oxygen concentration increases causing the soot particle radiation to disappear and the main radiating zone moves integrally toward the fuel side. At the same Z_{st}, the radiation area is broadened and the soot particle radiation is gradually enhanced.

Author Contributions: C.W. performed the data analysis and wrote the manuscript; G.T. and H.Y. contributed to the numerical calculation; L.L. and X.Y. reviewed the manuscript; Z.L. made the charts and performed analysis; C.L. contributed to the conception of the study and funded the data acquisition. All authors have read and agreed to the published version of the manuscript.

Funding: National Natural Science Foundation of China (51827808).

Institutional Review Board Statement: Not applicable.

Informed Consent Statement: Not applicable.

Data Availability Statement: Not applicable.

Conflicts of Interest: The authors declare no conflict of interest.

References

1. Buhre, B.J.P.; Elliott, L.K.; Sheng, C.D.; Gupta, R.P.; Wall, T.F. Oxy-fuel combustion technology for coal-fired power generation. *Prog. Energy Combust. Sci.* **2005**, *31*, 283–307. [CrossRef]
2. Wall, T.F. Combustion processes for carbon capture. *Proc. Combust. Inst.* **2007**, *31*, 31–47. [CrossRef]
3. Zheng, C.G.; Liu, Z.H. *Oxy-Fuel Combustion: Fundamentals, Theory and Practice*; Academic Press: Cambridge, MA, USA, 2018.
4. Li, S.Q.; Yu, Y.; Gao, Q. Measurements and modelling of oxy-fuel coal combustion. *Proc. Combust. Inst.* **2019**, *37*, 2643–2661. [CrossRef]
5. Abdelaal, M.; El-Riedy, M.; El-Nahas, A.M.; El-Wahsh, F.R. Characteristics and flame appearance of oxy-fuel combustion using flue gas recirculation. *Fuel* **2021**, *297*, 120775. [CrossRef]
6. Gopan, A.; Kumfer, B.M.; Phillips, J.; Thimsen, D.; Smith, R.; Axelbaum, R.L. Process design and performance analysis of a Staged, Pressurized Oxy-Combustion (SPOC) power plant for carbon capture. *Appl. Energy* **2014**, *125*, 179–188. [CrossRef]
7. Koohestanian, E.; Shahraki, F. Review on principles, recent progress, and future challenges for oxy-fuel combustion CO_2 capture using compression and purification unit. *J. Environ. Chem. Eng.* **2021**, *9*, 105777. [CrossRef]
8. Karataş, A.E.; Gülder, Ö.L. Soot formation in high pressure laminar diffusion flames. *Prog. Energy Combust. Sci.* **2012**, *38*, 818–845. [CrossRef]
9. Johansson, R.; Leckner, B.; Andersson, K.; Johnsson, F. Influence of particle and gas radiation in oxy-fuel combustion. *Int. J. Heat Mass Transf.* **2013**, *65*, 143–152. [CrossRef]
10. Wang, Y.; Chung, S.K. Soot formation in laminar counterflow flames. *Prog. Energy Combust. Sci.* **2019**, *74*, 152–238. [CrossRef]
11. Lou, C.; Chen, C.; Sun, Y.; Zhou, H. Review of soot measurement in hydrocarbon-air flames. *Sci. China Technol. Sci.* **2010**, *53*, 2129–2141. [CrossRef]
12. Li, Z.; Zhang, L.; Lou, C. In-situ measurement of soot volume fraction and tem- perature in axisymmetric soot-laden flames using TR-GSVD algorithm. *IEEE Trans. Instrum. Meas.* **2021**, *70*, 5001212.
13. Du, J.; Axelbaum, R.L. The effect of flame structure on soot-particle inception in diffusion flames. *Combust. Flame* **1995**, *100*, 367–375. [CrossRef]
14. Guo, Z.; Lou, C.; Liu, Z.D.; Zhou, H.C. The impact of combustion characteristics and flame structure on soot formation in oxy-enhanced and oxy-fuel diffusion flames. *Sci. China Technol. Sci.* **2013**, *56*, 1618–1628. [CrossRef]
15. Johnson, P.R.; Chakrabarty, R.K.; Kumfer, B.M. A modeling approach for soot formation in non-premixed flames with elevated stoichiometric mixture fraction. *Combust. Flame* **2021**, *229*, 111383. [CrossRef]
16. Lou, C.; Chen, X.B.; Yan, W.J.; Tian, Y.F.; Kumfer, B.M. Effect of stoichiometric mixture fraction on soot fraction and emission spectra with application to oxy-combustion. *Proc. Combust. Inst.* **2019**, *37*, 4571–4578. [CrossRef]
17. Lou, C.; Li, Z.; Zhang, Y.; Kumfer, B.M. Soot formation characteristics in laminar coflow flames with application to oxy-combustion. *Combust. Flame* **2021**, *227*, 371–383. [CrossRef]
18. Atreya, A.; Mungekar, H.P. Flame radiation and soot emission from partially premixed methane counterflow flames. *J. Heat Transf.* **2006**, *128*, 361–367.
19. Liu, F.; Guo, H.; Smallwood, G.J.; Mouna, E.H. Effects of gas and soot radiation on soot formation in counterflow ethylene diffusion flames. *J. Quant. Spectrosc. Radiat. Transf.* **2002**, *84*, 501–511. [CrossRef]
20. Lutz, A.E.; Kee, R.J.; Grcar, J.F.; Rupley, F.M. *OPPDIF: A FORTRAN Program for Computing Opposed-Flow Diffusionflames*; Sandia Report SAND96-8243; Sandia National Laboratories: Albuquerque, NM, USA, 1997.
21. Kee, R.J.; Rupley, F.M.; Miller, J.A. *CHEMKIN II: A Fortran Chemical Kinetics Package for the Analysis of Gas Phase Chemical Kinetics*; Sandia Report SAND89-8009B; Sandia National Laboratories: Albuquerque, NM, USA, 1989.
22. Gordon, S.; McBride, B.J. *Computer Program for Calculation of Complex Chemical Equilibrium Compositions and Applications*; National Aeronautics and Space Administration, Office of Management, Scientific and Technical Information Program: Washington, DC, USA, 1996.
23. Wang, H.; Frenklach, M. A detailed kinetic modeling study of aromatics forma- tion in laminar premixed acetylene and ethylene flames. *Combust. Flame* **1997**, *110*, 173–221. [CrossRef]
24. Appel, J.; Bockhorn, H.; Frenklach, M. Kinetic modeling of soot formation with detailed chemistry and physics: Laminar premixed flames of C2 hydrocarbons. *Combust. Flame* **2000**, *121*, 122–136. [CrossRef]
25. Frenklach, M.; Wang, H. *Soot Formation in Combustion: Mechanisms and Models*; Springer: Berlin/Heidelberg, Germany, 1994.
26. Abu-Romia, M.M.; Tien, C.L. Appropriate mean absorption coefficients for infrared radiation of gases. *J. Heat Transf.* **1967**, *89*, 321. [CrossRef]
27. Grosshandler, W.L. *RADCAL: A Narrow-Band Model for Radiation Calculations in a Combustion Environment*; NIST Technical Note 1402; National Institute of Standards and Technology: Gaithersburg, MA, USA, 1993.
28. Kent, J.H.; Honnery, D.R. A soot formation rate map for a laminar ethylene diffusion flame. *Combust. Flame* **1990**, *79*, 287–299. [CrossRef]

29. Kang, K.T.; Hwang, J.Y.; Chung, S.H.; Lee, W. Soot zone structure and sooting limit in diffusion flames: Comparison of counterflow and co-flow flames. *Combust. Flame* **1997**, *109*, 266–281. [CrossRef]
30. Choi, B.C.; Choi, S.K.; Chung, S.H.; Kim, J.S.; Choi, J.H. Experimental and numerical investigation of fuel mixing effects on soot structures in counterflow diffusion flames. *Int. J. Auto. Tech.* **2011**, *12*, 183–191. [CrossRef]
31. Xu, L.; Yan, F.; Zhou, M.; Wang, Y.; Chung, S.H. Experimental and soot modeling studies of ethylene counterflow diffusion flames: Non-monotonic influence of the oxidizer composition on soot formation. *Combust. Flame* **2018**, *197*, 304–318. [CrossRef]
32. Wang, Y.; Chung, S.H. Formation of soot in counterflow diffusion flames with carbon dioxide dilution. *Combust. Sci. Tech.* **2016**, *188*, 805–817. [CrossRef]
33. Li, Z.; Amin, H.M.F.; Liu, P.; Wang, Y.; Chung, S.H.; Roberts, W.L. Effect of dimethyl ether (DME) addition on sooting limits in counterflow diffusion flames of ethylene at elevated pressures. *Combust. Flame* **2018**, *197*, 463–470. [CrossRef]
34. Tang, Q.; Wang, M.; You, X. Measurements of sooting limits in laminar premixed burner-stabilized stagnation ethylene, propane, and ethylene/toluene flames. *Fuel* **2019**, *235*, 178–184. [CrossRef]
35. Barlow, R.S.; Karpetis, A.N.; Frank, J.H.; Chen, J.Y. Scalar profiles and NO formation in laminar opposed-flow partially premixed methane/air flames. *Combust. Flame* **2001**, *127*, 2102–2118. [CrossRef]